Applied Catalysis B: Environmental 304 (2022) 121017

Contents lists available at ScienceDirect

Applied Catalysis B: Environmental

journal homepage: www.elsevier.com/locate/apcatb

Highly efficient disinfection based on multiple enzyme-like activities of Cu_3P nanoparticles: A catalytic approach to impede antibiotic resistance

Daiyong Chao [a,b], Qing Dong [a,b], Jinxing Chen [b], Zhixuan Yu [b], Weiwei Wu [b], Youxing Fang [b], Ling Liu [b,*], Shaojun Dong [a,b,**]

[a] College of Chemistry, Jilin University, Changchun 130012, PR China
[b] State Key Laboratory of Electroanalytical Chemistry, Changchun Institute of Applied Chemistry, Chinese Academy of Sciences, Changchun 130022, PR China

ARTICLE INFO

Keywords:
Cu_3P NPs
Super antibacterial efficiency
Bacterial resistance
Fishery disinfection
Wound healing

ABSTRACT

Cu_3P nanoparticles (NPs) were proposed as an efficient antibacterial agent for impeding bacterial resistance. Both sensitive and resistant strains of *E. coli* and *S. aureus* (3×10^6 CFU mL^{-1}), and the microbial populations from a fishery water were completely inactivated by Cu_3P NPs (≤ 1.5 μg mL^{-1}) within 30 min with no regrowth. The antibacterial mechanism of Cu_3P NPs relied on their own multiple enzyme-like activities, to elucidate, the action of ROS produced by their oxidase- and peroxidase- like activities was facilitated by their inherent activities for glutathione depletion and the lipid peroxidation. Comparing with that traditional antibiotics induced bacterial resistance (6 out of 7) within 3 passages, Cu_3P NPs kept their initially inactivated efficiency, demonstrating that they can delay the onset of bacterial resistance. Furthermore, the Cu_3P NPs shown no obviously toxic effect on aquatic organisms and a negligible side-effect toward mammalian tissues. This strategy is insightful for struggle with resistant bacteria.

1. Introduction

Bacterial resistance has been evolved with the continual applications of antibiotics. To conquer the limitations of traditional antibiotic, great efforts have been committed towards the evolution of alternative strategies [1–5]. Recently, various nano-antibacterial agents have emerged due to their particular antibacterial mechanisms, which are summarized as that: the physical contact, such as graphene-based materials [6,7]; the metal ions and ligands release, such as Ag ions [8]; the oxidative stress, such as the oxidase (OXD) and peroxidase (POD) mimics [9–12]; the photothermal/photodynamic effect, such as Ti- and Mo-based nanomaterials [13–17]; and the synergistic effect with multiple above mechanisms [18,19]. Theoretically, these antibacterial mechanisms can largely escape from the resistance mechanisms of the traditional antibiotics that mostly interfere the syntheses of DNA and RNA as well as their encoded proteins.

Although a lot of nano-antibacterial agents have been reported, there still remains a big gap between laboratory investigations and practical applications [20]. For boosting the practical applications of nano-antibacterial agents, following issues should be explored clearly. 1) How can nano-antibacterial agents effect the produce and the spread of resistant bacteria, which has not been precisely and sufficiently investigated [21]. 2) Most of the previous nano-antibacterial agents require the auxiliary conditions that may damage the healthy tissues, such as the photo- or electro- or thermal or chemical (H_2O_2 for POD mimic) mediated antibacterial reactions [22]. 3) So far, expect some photocatalytic materials have been used for the inactivation of real water samples [23–25], most studies on the nano-antibacterial agents are still based on a few laboratorial bacteria, such as *Escherichia coli* (*E. coli*), *Staphylococcus aureus (S. aureus)*, *Salmonella typhimurium* (*S. typhimurium*) and so forth, but rarely for the populations in the natural environments [26,27]. 4) The acidic conditions (pH 3–4) are required by the most developed OXD and POD mimics, which restrict their applications under the near-neutral pH conditions [28–30]. Therefore, more decent experimental designs are required to address the above issues [31].

Besides, a particularly important thing is that the current applications of nano-antibacterial agents are mainly focused on human-related aspects, but the largest consumption of antibacterial agents in cultivation and breeding industries has been neglected [32]. More recently,

* Corresponding author.
** Corresponding author at: Changchun Institute of Applied Chemistry, Chinese Academy of Sciences, Changchun 130022, PR China.
E-mail addresses: liuling@ciac.ac.cn (L. Liu), dongsj@ciac.ac.cn (S. Dong).

https://doi.org/10.1016/j.apcatb.2021.121017
Received 21 September 2021; Received in revised form 25 November 2021; Accepted 14 December 2021
Available online 16 December 2021

certain types of inorganic nanoparticles (NPs) have been developed for practical disinfection applications, mainly including metal and metal oxides ($nTiO_2$, ZnO, nAg, nCu, CuO_x, and so forth) [33,34]. Among them, CuO_x NPs show a potential application in the complex water samples based on their broad-spectrum antibacterial activity [35]. Herein, we found that the antibacterial efficiency of CuO_x NPs can be significantly enhanced by a phosphatization process to form Cu_3P NPs. The as-prepared Cu_3P NPs shown a super antibacterial activity towards the antibiotic resistant bacteria (ARB) and real fishery water sample. The antibacterial mechanism of Cu_3P NPs relied on their multiple enzyme-like activities. Furthermore, an ARB and antibiotic resistant gene (ARG)-inducing experiment was designed for investigating the bacterial resistance of Cu_3P NPs.

2. Experiment section

2.1. Materials and instrumentation

Glutathione (GSH), o-phenylenediamine (OPD), sodium hypophosphite (NaH_2PO_2) and sopropyl alcohol (IPA) were purchased from Aladdin. Terephthalic acid (TA), 5,5′-dithiobis (2-nitrobenzoic acid) (DTNB) and 30% H_2O_2 were provided from Beijing Chemical Works. Catalase, superoxide dismutase (SOD), histidine, and 2′,7′-dichlorofluorescin diacetate (DCFH-DA) were obtained from Sigma-Aldrich. LIVE/DEAD™ BacLight™ Bacterial Viability Kit (L13152) was purchased from Thermo Fisher.

The morphologies of Cu_3P NPs and bacteria were characterized by a field emission scanning electron microscopy (SEM, Hitachi, SU-8020) and a transmission electron microscope (TEM, FEI Tecnai G2 F20). X-ray diffraction (XRD) patterns were obtained on a Bruker D8 Advance diffractometer using Cu Kα radiation. X-ray photoelectron spectroscopy (XPS) measurements were performed on a PHI 5000 Versa Probe (ULVAC-PHI). Absorption spectra and fluorescence spectra were recorded by using a Cary 60 UV–vis spectrophotometer (Varian) and a Cary Eclipse fluorescence spectrophotometer (Agilent Technologies), respectively. The bacteria in LIVE/DEAD assay were imaged by confocal laser scanning microscopy (CLSM, Nikon, C2, Japan). The radical active species were investigated by electron spin resonance (ESR) spectra detected on Bruker EMX PLUS with the following parameters: center field 3502.00 G, sweep width 100.0 G and power 6.325 mW.

2.2. Preparation and characterizations of Cu_3P NPs

CuO NPs were prepared according to a previous method [36]. For preparing Cu_3P NPs, 20 mg CuO NPs and 300 mg NaH_2PO_2 were placed at two separate positions in a porcelain boat with NaH_2PO_2 at the upstream side of the furnace. The samples were heated to 300 °C for 2 h with a heating rate of 5 °C min^{-1} under N_2 atmosphere. Finally, the prepared Cu_3P NPs were washed with deionized water and ethanol.

The OXD-like activity of Cu_3P NPs was measured by colorimetric assays based on the OPD substrate. The final concentrations of 10 μg mL^{-1} Cu_3P NPs, 1.5 mM OPD and 100 mM Tris-HCl buffer medium (pH 7.0) were mixed and incubated under 37 °C. As the substrate added, the absorbance at 450 nm was monitored. The POD-like activity of Cu_3P NPs was measured based on the above tests by adding H_2O_2. The influence of pH values on the enzyme-like activity was measured in different buffer solutions. The oxidation ability of Cu_3P NPs to GSH was quantified using Ellman's assay. Typically, 225 μL of Cu_3P NPs dispersion (40 μg mL^{-1}) was added into GSH (225 μL, 0.8 mM) bicarbonate buffer solution (50 mM, pH 8.6). After incubation in dark condition, 785 μL of Tris-HCl (50 mM, pH 8.5) and 15 μL of DTNB (100 mM) were added into the mixtures. To remove Cu_3P NPs, the mixtures were filtered with a 0.22 μm filter membrane. The absorbance of supernatant at 412 nm was monitored by a microplate spectrophotometer.

2.3. Antibacterial experiment and bacterial characterization

E. coli (ATCC25922 and DH5α), *Staphylococcus aureus* (*S. aureus* ATCC6538) and methicillin-resistant *S. aureus* (MRSA ATCC43300) were brought from Beijing Microbiological Culture Collection Center and cultured by Luria-Bertani (LB) medium and nutrient broth medium. The sensitive bacteria were only used as the control species. A single bacterial colony was cultured in 20 mL of medium under 37 °C for shaking 12 h. The as-cultured bacteria were then washed and diluted by PBS for final concentration of 3×10^6 colony-forming units (CFU) mL^{-1} that were treated with a series dose of Cu_3P NPs under the laboratory conditions. After treatment with different times, the bacterial suspensions were diluted to 10^3 CFU mL^{-1} with PBS, and then spread on the nutrient agar plate and incubated under 37 °C for 24 h for CFU counting. The levels of lipid peroxidation (LPO) and glutathione of the bacteria were measured by using a Micro-malondialdehyde (MDA) Assay Reagent Kit and a GSH and GSSG Assay Kits, respectively.

After the antibacterial assays, the bacteria were collected by centrifugation and fixed with glutaraldehyde (2.5%) for 4 h at 4 °C under dark conditions, followed by sequential dehydrating with 30%, 50%, 70%, 80%, 90%, and 100% of ethanol for 10 min, respectively. After sputter-coating with gold, the bacterial morphology was characterized by SEM. TEM characterizations of bacterial ultrathin sections were operated according to our previous work [37]. For LIVE/DEAD assay, the tested bacteria were collected and stained with SYTO 9 and propidium iodide (PI) for 15 min in the dark and visualized by a confocal fluorescence microscopy. A regrowth test was carried out by seeding the treated bacteria back to the fresh medium.

2.4. Detection of reactive oxygen species (ROS)

(a) The generation of the •OH, $•O_2^-$ and $^1O_2$ radicals was determined by ESR technique according to previous reports [38,39]. (b) For the in vitro antibacterial test, catalase (30 U mL^{-1}), IPA (0.1 mM), and SOD (30 U mL^{-1}) were used for trapping the H_2O_2, hydroxyl radicals (•OH), and superoxide radical anion ($•O_2^-$), respectively. (c) For the detection of •OH generated by H_2O_2 (by POD-like activities), TA was used as a fluorescent probe for the detection of •OH. Briefly, the mixtures composed of Cu_3P NPs (10 μg mL^{-1}), H_2O_2 (40 mM) and terephthalic acid (TA, 5 mM) were incubated at 37 °C for 2 h, and the fluorescence intensity (Ex 312 nm/Em 425 nm) was recorded. (d) For the in vivo detection, the overall intracellular ROS level was investigated by using DCFH-DA fluorescent probe. After treatments, bacteria were stained with 10 μM DCFH-DA for 30 min in the dark at room temperature and washed with PBS twice. The fluorescence intensity was measured by a fluorescent spectrophotometer.

2.5. Wound model and histological analysis

MASA-infected mice (6–8 weeks, 18–21 g) wound model was built to assess the in vivo antibacterial activity of Cu_3P NPs. After anesthesia, a wound (~ 78 mm^2) was created on the mice back by surgical procedure and infected with MRSA (50 μL, 10^7 CFU mL^{-1}). After 24 h infection, all tested mice were divided into three groups (with five per group): PBS, Cu_3P NPs (5 μg mL^{-1}) and Cu_3P NPs (5 μg mL^{-1}) + H_2O_2 (50 μM). The wounds were photographed at 24 h intervals. The mice were treated at fifth day and the wound tissues were collected. After incubation for 24 h at 37 °C, the amount of CFUs in the suspensions was determined. Animal studies were conducted under the guidelines of the Institutional Animal Care and Use Committee. For histological analysis, the wounds of each group were harvested at day 5 and placed in 4% paraformaldehyde solution. Then the wounds were embedded in paraffin for Hematoxylin-Eosin (HE) staining.

2.6. ARGs analysis and ARB-inducing experiments

The real water sample from a local fishery was employed as a gene bank to investigate the bacterial resistance. ARGs analysis was carried out by high-throughput sequencing (HTS) technique. A detailed description of the total DNA extraction, polymerase chain reaction (PCR) amplification, sequencing, and data processing were mainly referenced the previous study [40,41]. The HTS was performed on a NovaSeq platform (Illumina, USA). The raw reads were demultiplexed and quality-filtered by using QIIME (v1.9.1) in accordance with the previous report [42]. Bowtie2 was used to compare Clean Reads of each sample with non-redundant gene sets. Samtools was used to count the number of reads on each gene being compared and calculate the gene abundance. ARGs were annotated by using the database https://card.mcmaster.ca/download. For the MGE analysis, the database for integrase genes from the INTEGRALL database (http://integrall.bio.ua.pt/), ISs sequences from the ISfineder database (https://www-is.biotoul.fr/), and plasmid sequences from the NCBI plasmid genome database (ftp://ftp.ncbi.-nih.gov/genomes/Plasmids/) were adopted.

The equal values of real water sample were seeded on the nutrient plates with a series of antibiotic concentrations. The minimum inhibitory concentration (MIC) for each antibiotic was recorded at the last plate with the naked-eye readout colonies. The colonies on the plate with MIC antibiotics were further seeded for 3 passages by the same tested antibiotic. Then, the survived bacteria for each antibiotic were seeded on the nutrient plates with an over MIC of the antibiotics. The parallel experiment was carried out for Cu_3P NPs.

2.7. Biosafety evaluation

The cytotoxicity of Cu_3P NPs was studied via a standard Cell Counting Kit-8 (CCK-8) assay by using MCF-7 and HepG2 cells as the tested cells. The cells in DMEM medium with 10% fetal bovine serum (100 μL, about 5000 cells/well, five wells for each concentration) were seeded in 96-well plate for 24 h. Then, the cells were incubated with a series of concentrations of Cu_3P NPs. After 24 h incubation, CCK-8 solution was added into each well and incubated for another 1 h. Finally, the absorbance at 450 nm was measured by a microplate reader for evaluating the cell viability.

PBS or Cu_3P NPs (5 mg kg^{-1}, 100 μL) were intravenously injected

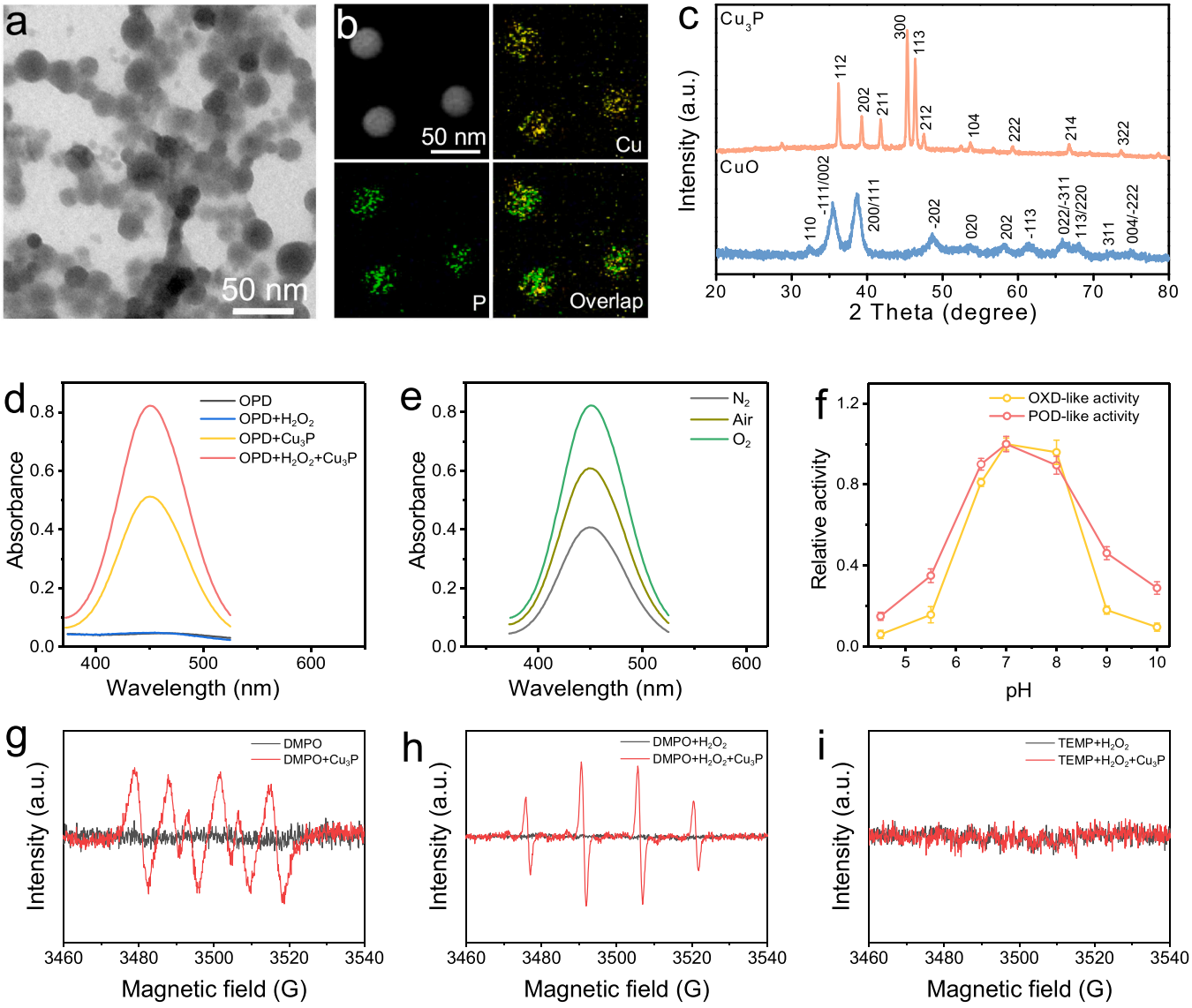

Fig. 1. Characterizations and properties of Cu_3P NPs. (a) TEM image. (b) Dark-field TEM image and corresponding elemental mapping. (c) XRD patterns. (d) OXD- and POD-like properties. (e) Effect of different saturated gases on the OXD-like activity. (f) pH-dependent OXD- and POD-like activities. ESR spectra of the DMPO+Cu_3P NPs methanol suspension (g), DMPO + H_2O_2 + Cu_3P NPs aqueous suspension (h), TEMP + H_2O_2 + Cu_3P NPs aqueous suspension (i).

into the mice. At the fifth day after injection, the mice were sacrificed to collect blood samples for biochemistry assay. Meanwhile, the major organs (heart, liver, spleen, lung and kidney) of these mice were harvested and fixed in 4% paraformaldehyde solution for histological examination through H&E staining.

3. Results and discussion

3.1. Characterization of Cu_3P NPs

3.1.1. Morphology and crystal structure

CuO NPs (Fig. S1) were prepared via a facile chemical precipitation route, which subsequently underwent a low-temperature phosphatization process to convert into Cu_3P NPs (Fig. 1a). The Cu and P elements were homogeneously distributed in the sphere Cu_3P NPs (Fig. 1b). In the XRD patterns (Fig. 1c), all characteristic diffraction peaks of CuO NPs and Cu_3P NPs were indexed to those of the standard pattern JCPDS Nos. 80-1916 and 71-2261 [36,43]. XPS was further applied to analyze the chemical states of Cu and P elements in Cu_3P NPs. In the high-resolution Cu 2p and P 2p spectra (Fig. S2), the peaks at 932.5 eV (Cu $2p_{3/2}$) and 128.9 eV (P 2p) were typical peaks of Cu_3P NPs, and the peaks at 934.8 eV (Cu $2p_{3/2}$), 954.3 eV (Cu $2p_{1/2}$), and 133.8 eV (P 2p) were caused by the superficial oxidation of the Cu_3P NPs in air [44,45]. These results indicated that Cu_3P NPs were prepared successfully.

3.1.2. Catalytic activities

The catalytic properties of the Cu_3P NPs were investigated by using OPD as the chromogenic substrate. As shown in Fig. 1d and e, OPD was catalyzed by Cu_3P NPs in the absence of H_2O_2 and the catalytic activity was dependent on oxygen concentration, indicating the OXD-like activity of Cu_3P NPs. The OXD-like activity of Cu_3P NPs was pH-related and exhibited the highest value at pH 7.0 (Fig. 1f), which was different from the previously reported OXD mimics that required the acid conditions. Then, the OXD-like activity of the Cu_3P NPs was further studied by Michaelis-Menten constant (K_m) and maximum initial velocity (V_{max}). In Fig. S3, the low K_m value (0.95 mM) suggested the high affinity of Cu_3P NPs for substrates. The V_{max} value 0.94×10^{-8} M s^{-1} was higher than that of previous OXD mimics, meaning a high OXD-like property of the present materials [46,47]. When H_2O_2 was added into the Cu_3P NPs/OPD reaction system, the absorbance at 450 nm was increased significantly (Fig. 1d), indicating a POD-like activity of Cu_3P NPs. Interestingly, the Cu_3P NPs exhibited high POD-like activity over a pH range of 6.5–8.0 (Fig. 1f), which was different from the pH range 3.0–4.0 required by the most previously reported POD mimics. Additionally, the $\bullet O_2^-$ and the •OH were detected by ESR technique (Fig. 1g, h), but no $^1O_2$ was detected (Fig. 1i) [39]. The intrinsic properties of these enzyme-like activities could be used for ROS generation that was able to seriously impair the membrane integrity of bacteria, and thus leading to a predictable antibacterial capability of the present Cu_3P NPs.

3.2. Antibacterial activity of Cu_3P NPs

Encouraged by the capability of Cu_3P NPs for ROS generation, their antibacterial properties were then examined. The antibacterial performance of the present Cu_3P NPs was really preferred by comparing with the other metal phosphides (Table S1 and Fig. S4). Five sizes of Cu_3P NPs were prepared from different precursors of CuO and $Cu(OH)_2$ (Fig. S5) and their antibacterial activities shown no statistical difference (Fig. S6), indicating the good reproducibility of the Cu_3P NPs antibacterial performance. The dose (Fig. S7) and time (Fig. 2a) for the system were further optimized. As shown in Fig. 2a, inactivation efficiency for both Gram-negative bacteria *E. coli* and Gram-positive bacteria MRSA was achieved to > 99.9% by Cu_3P NPs within 20 min with 1.5 and 0.5 μg mL^{-1}, respectively. The minimum valid concentrations were significantly lower than that of their precursor CuO NPs (Fig. S8). The inactive period by using Cu_3P NPs was further shortened to 15 min by adding a low dosage H_2O_2 (100 μM in Fig. S9). The traditional therapeutic concentrations of 0.5–3% H_2O_2 are still high to damage normal

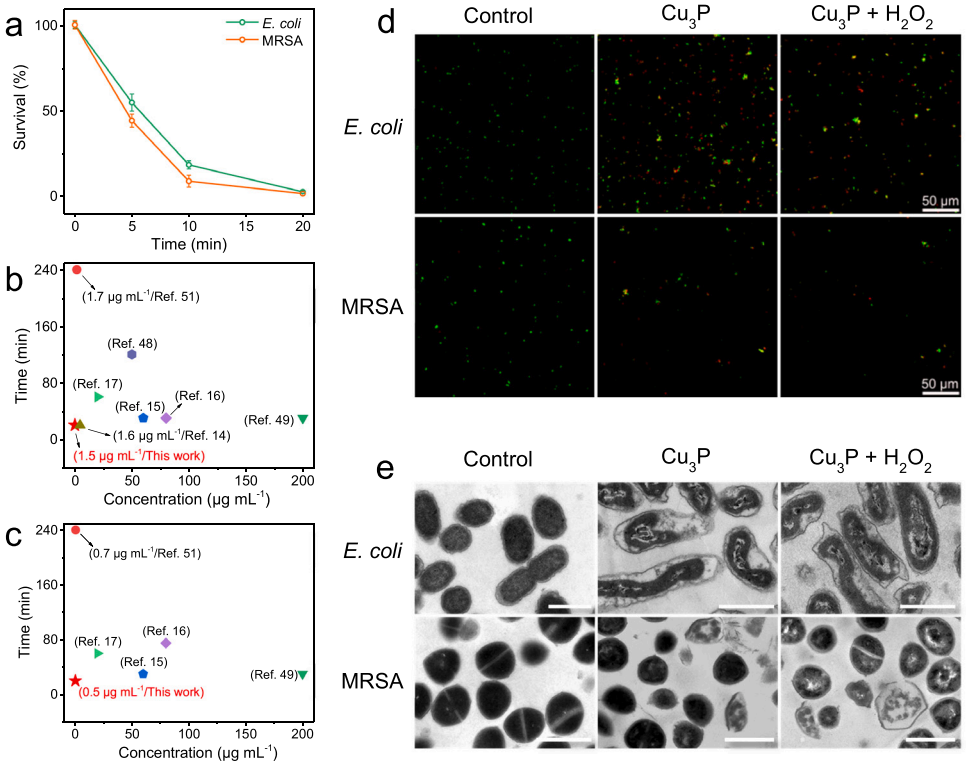

Fig. 2. Antibacterial property of Cu_3P NPs. (a) Time-dependent inactivation efficiency of *E. coli* (3×10^6 CFU mL^{-1}) and MRSA (3×10^6 CFU mL^{-1}) treated by Cu_3P NPs with the concentrations of 1.5 and 0.5 μg mL^{-1}, respectively. Antibacterial properties of Cu_3P NPs and the previously reported nanomaterials toward (b) *E. coli* and (c) MRSA. (d) Fluorescence merge images in LIVE/DEAD assay. (e) TEM images of the bacterial ultrathin sections. Bars: 1 μm.

tissues in the bacterial disinfection process and the low dosage of H_2O_2 in the present work is beneficial for minimizing the damage [48,49]. To our best knowledge, this is one of the most efficient antibacterial agents that does not need auxiliary conditions, even can compare with the light-mediated ones (Fig. 2b, c) and the commercial Ag NPs (Fig. S10).

To evaluate the injury of the bacterial cells, the bacterial morphologies were characterized by SEM and the permeability of cell membrane was assessed by LIVE/DEAD assay, where SYTO 9 was used to label the live microbes and propidium iodide (PI) for the dead ones. As shown in Fig. 2d, almost all bacterial cells were stained by PI in the Cu_3P NPs- and Cu_3P NPs/H_2O_2-treated groups in the LIVE/DEAD assay (raw images in Fig. S11). These bacterial cells became wrinkled and rough (Fig. S12), and their cell membranes and cell walls were seriously damaged (Fig. 2e). The regrowth test also demonstrated the complete inactivation of these bacteria by the present approach (Fig. S13). The present results indicated that these bacteria were sacrificed at the end stage of bacterial membrane permeabilization under the Cu_3P NPs actions.

3.3. Disinfection mechanism of Cu_3P NPs

In a previous report, the intracellular uptake of Cu^{2+} released from Cu-containing materials is responsible for their antibacterial activity [50]. However, in this work, the Cu_3P NPs supernatant that was set for 1 week to release Cu^{2+} showed no obvious antibacterial activities toward both *E. coli* and MRSA (Fig. S14). In order to further eliminate the possibility of Cu^{2+} sterilization in the antibacterial experiments, the concentration of Cu^{2+} released from Cu_3P NPs was quantitatively investigated by inductively coupled plasma optical emission spectroscopy (ICP-OES). In the present Cu_3P NPs supernatant, 10.5 ppb of Cu^{2+} was determined. A same concentration of Cu^{2+} prepared by $CuCl_2$ shown negligible antibacterial activities (Fig. S15). This result indicated that the antibacterial efficiency of Cu_3P NPs mostly do not rely on their released Cu^{2+}.

ROS are commonly used to explain the antibacterial mechanism for OXD- and POD-like nanomaterials [51,52]. Herein, catalase, IPA, SOD and histidine were used as the scavengers to trap the H_2O_2, •OH, $•O_2^-$, and $^1O_2$, respectively. As shown in Fig. S16, the antibacterial capability was inhibited by adding SOD, indicating that $•O_2^-$ had mainly defined the antibacterial activity of Cu_3P NPs, it was accordant with the ESR results. Besides, since the antibacterial efficiency was enhanced by adding H_2O_2, TA probe was employed to detect •OH (Fig. S17) and the result indicated that the POD-like activity of Cu_3P NPs played antibacterial act by releasing •OH. In addition, the DCFH-DA probe shown that the ROS levels in the bacterial cells treated by Cu_3P NPs were higher than that in the control cells (Fig. 3a, b), which were accordant to the antibacterial results. In the intracellular MDA test, the LPO was increased by Cu_3P NPs to 3.6 and 2.6 fold for *E. coli* and MRSA, respectively (Fig. 3c). Combined with the LIVE/DEAD assay (Fig. 2e), the LPO activity had promoted the permeability of bacterial membrane and facilitated the transmembrane transports of ROS, and the inactivation efficiency of Cu_3P NPs was therefore enhanced [53].

On the other hand, the antioxidants, mainly GSH (0.1–10 mM) in the bacterial cells, can directly neutralize ROS and diminish the antibacterial efficiency [54]. Herein, Ellman's assay was performed to quantify the GSH oxidation by Cu_3P NPs (Fig. S18). After 1.5 h incubation, 85.54% oxidation ratio was obtained and a near-depletion could be

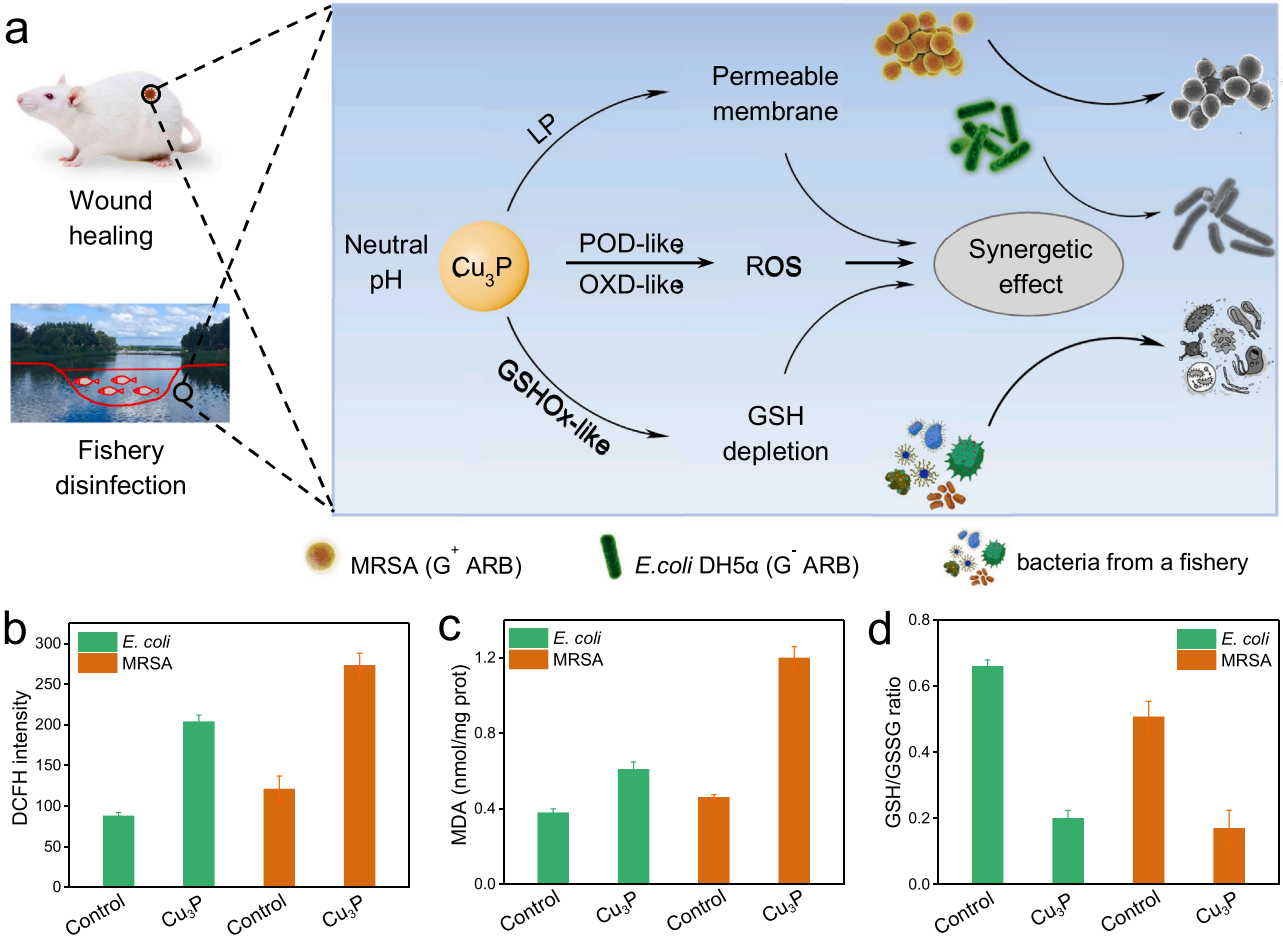

Fig. 3. Antibacterial mechanism of Cu_3P NPs. (a) Schematic diagram illustrating Cu_3P NPs for MRSA -infected wound healing and fishery disinfection. (b) ROS levels, (c) LPO and (d) GSH/GSSG ratios in *E. coli* and MRSA for Cu_3P NPs treating experiments.

expected with the prolonging of incubation time. Beyond that, the ratios of intracellular GSH/GSSG were decreased from 0.65 for *E.coli* and 0.5 for MRSA to about 0.2 for both bacteria (Fig. 3d). The present results indicated that GSH depletion by Cu_3P NPs alleviated the bacterial antioxidant capability and rendered the bacteria more vulnerable to ROS-dependent oxidative stress. To summarize the above results, the GSH depletion and the permeable bacterial membrane worked together to facilitate the ROS-based antibacterial actions. In a previous work, Cu_3P nanowires were used as the electrode-modified materials to enhance the electroporation guarantees for a disinfection application [55]. In this work, we argue for that Cu_3P NPs themselves are antibacterial agents based on the synergetic effects of their multiple enzyme-like activities.

3.4. Bacterial resistance of Cu_3P NPs

The aquaculture industry is inevitable to use a mass of antibacterial agents for disinfection, which induces bacterial resistance and results in the rapid emergence and dissemination of ARB and ARG [56,57]. Herein, the bacterial resistance to antibacterial agents was investigated by using a local fishery water sample (Fig. 4a). To know the bacterial antibiotic resistance in the fishery, a large-scale field sampling and HTS analysis were carried and the top 19 ARG sub-types were mainly assigned to 7 classifications (Fig. 4b). In this work, these ARG types were investigated by employing erythromycin, bacitracin, streptomycin sulfate, penicillin, tetracycline HCl, and vancomycin as the representative antibiotics (excluding multidrug, Table S2). Rifampicin was used to assess the one that without resistant genes annotated from the raw sample.

For the fishery water sample (the genera annotated by HTS were listed in Supplementary Material Total genera), a completely disinfected efficiency was achieved within 30 min with 0.8 μg mL^{-1} Cu_3P NPs (Figs. S19a and 20a). This dose was significantly lower than that of the commercial antibacterial agent, where over 30 μg mL^{-1} Ag NPs were needed under the same conditions (Figs. S19b and 20b). For these tested antibiotics, as shown in Fig. 4c–e, the MIC was recorded as the dose of an antibiotic on the last plate with survival bacteria. After 3 passages of the inducing experiments, the survival ratios of the bacteria on the plates contained six test antibiotics were significantly enhanced. However, the Cu_3P NPs and the rifampicin that without resistance genes had kept their antibacterial capacities (Fig. 4e). The present results indicated that Cu_3P NPs could be an effective strategy to impede the problem of antibiotic abuse in the aquaculture industry.

The above results suggested that the antibiotic power for the present fishery has become weak. It will be dangerous with the vertical transfer of ARGs by giving an enough passages of antibiotics process (Table S3). Combining with the horizontal gene transfer induced by some mobile genetic elements (MGEs) annotated by HTS from this fishery, there is a higher risk for ARGs propagation among the local population. Cu_3P NPs are able to elude the spread mechanism of ARGs and keep their antibacterial capability in certain passages. Therefore, Cu_3P NPs present a promising way for the critical ecosystems in this fishery. However, it was noticed that the bacterial resistances induced by the other nano-antibacterial agents were reported [58]. The same risk presumably could also be induced by the present Cu_3P NPs, if in a long-term and large-scale applications.

3.5. Biosafety of Cu_3P NPs

3.5.1. Aquatic biosafety

Based on the confirmation of the super antibacterial activity of Cu_3P NPs, their biosafety was then evaluated. As shown in Fig. 5a, after the

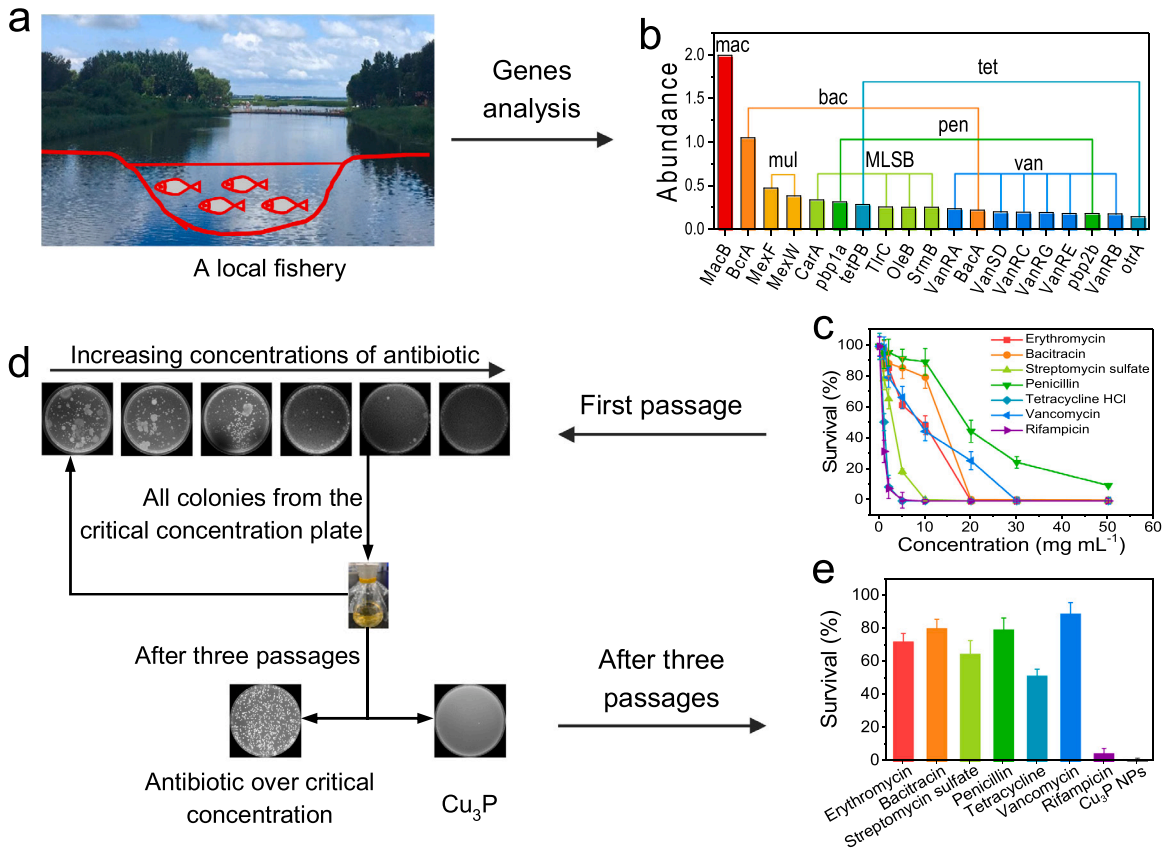

Fig. 4. Bacterial resistance and ARB-inducing experiment. (a) Photographs of the fishery and (b) the top 19 subtypes of ARGs annotated from this fishery water sample. (c) Survival rate of the bacteria from the real water sample treated with typical antibiotics and Cu_3P NPs in the first passage. (d) Schematic representation of the ARB-inducing experiment. (e) Survival rate of the bacteria after three passages.

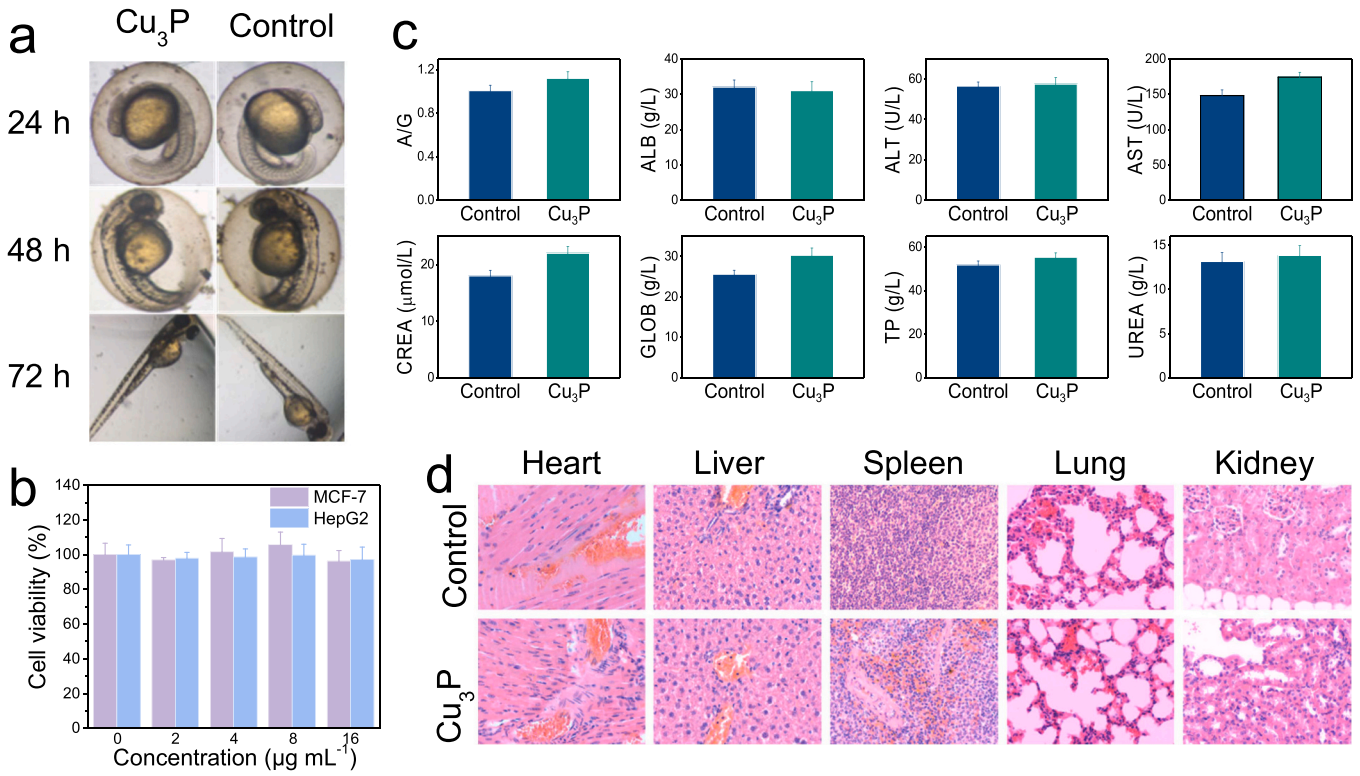

Fig. 5. Biosafety of Cu_3P NPs. (a) Toxic effects of Cu_3P NPs on zebrafish embryos. (b) Cell viabilities of MCF-7 and HepG2 cells treated by Cu_3P NPs. (c) Blood physiological index injected with Cu_3P NPs. (d) Photomicrographs of the major organs stained with H&E after Cu_3P NPs treatments.

incubation with Cu_3P NPs for 72 h, the zebrafish embryos had no show changes. This result indicated that there was no significant toxicity of Cu_3P NPs on zebrafish embryos at the test concentration and the materials were safe for aquatic life.

3.5.2. *Mammalian biosafety*

A standard Cell Counting Kit-8 (CCK-8) assay was carried out to evaluate the in vitro cytotoxicity of Cu_3P NPs. 16 μg mL^{-1} Cu_3P NPs (Fig. 5b) that was over tenfold concentration used in the antibacterial experiments (1.5 and 0.5 μg mL^{-1}) showed no significant toxicity toward MCF-7 and HepG2 cells. To investigate in vivo safety, Cu_3P NPs were intravenously injected into healthy mice. There were no obvious changes showed by the blood indicators (Fig. 5c) and no obvious toxicity toward the main organs by the histology analysis (Fig. 5d).

Based on the results of biosafety tests, the application of Cu_3P NPs was expanded to wound healing by using an MRSA-infected wound model. As shown in Fig. S21a, b, both Cu_3P NPs and Cu_3P NPs/H_2O_2 significantly promoted wound healing. The bacteria in the wound tissues were quantified and the CFU cultured from the Cu_3P NPs treated groups were obviously less than those from the control (Fig. S21c). The wound-healing efficiency was further evaluated by histological analyses and incomplete epidermal layer and inflammatory cells in both treated wounds were obviously less than those in the control group (Fig. S21d). The biosafety of Cu_3P NPs could also be reflected by the previous investigation on their application of tumor therapy [59]. These results demonstrated that Cu_3P NPs presented supper antibacterial activity and could promote wound repair.

4. Conclusions

In summary, we proposed that Cu_3P NPs were efficient nano-antibacterial agents and the antibacterial mechanism was explored as a synergetic effect by their multiple enzyme-like activities. It depended on the inactivation by ROS, which was further enhanced by the destruction of the defense system caused by the GSH depletion and the permeable cell membrane induced by LPO. The disinfected efficiency for a natural fishery water was achieved to 99.9% within 20 min without toxic effect on zebrafish embryos. For the fishery water, the delayed onset time of the bacterial resistance was demonstrated by comparing Cu_3P NPs to the conditional antibiotics in an ARB-inducing experiment. Moreover, in vivo and in vitro biosafety data indicated the Cu_3P NPs were hurtles in the present approach and a MRSA-infected wound healing was significantly accelerated. This work not only proposed an efficient antibacterial agent, but also provided a crucial proof for that the nano-antibacterial agents can reduce the bacterial resistance compared with the traditional antibiotics in a certain passages.

CRediT authorship contribution statement

Daiyong Chao: Conceptualization, Data curation, Formal analysis, Writing – original draft. **Qing Dong**: Resources, Methodology. **Jinxing Chen**: Methodology. **Zhixuan Yu**: Investigation, Methodology. **Weiwei Wu**: Validation. **Youxing Fang**: Validation. **Ling Liu**: Conceptualization, Writing – review & editing, Project administration. **Shaojun Dong**: Supervision, Funding acquisition.

Declaration of Competing Interest

The authors declare that they have no known competing financial interests or personal relationships that could have appeared to influence the work reported in this paper.

Acknowledgments

This work was financially supported by the Ministry of Science and Technology of China (No. 2016YFA0203203) and the National Natural Science Foundation of China (Nos. 22074137 and 21721003).

Appendix A. Supplementary material

Supplementary data associated with this article can be found in the online version at doi:10.1016/j.apcatb.2021.121017.

References

[1] M.J. Blaser, Antibiotic use and its consequences for the normal microbiome, Science 352 (2016) 544–545.
[2] T.S. Crofts, A.J. Gasparrini, G. Dantas, Next-generation approaches to understand and combat the antibiotic resistome, Nat. Rev. Microbiol. 15 (2017) 422–434.
[3] F. Gould, Z.S. Brown, J. Kuzma, Wicked evolution: can we address the sociobiological dilemma of pesticide resistance? Science 360 (2018) 728–732.
[4] E. Bakkeren, J.S. Huisman, S.A. Fattinger, A. Hausmann, M. Furter, A. Egli, E. Slack, M.E. Sellin, S. Bonhoeffer, R.R. Regoes, M. Diard, W.D. Hardt, Salmonella persisters promote the spread of antibiotic resistance plasmids in the gut, Nature 573 (2019) 276–280.
[5] X. Xie, R. Wang, X. Zhang, Y. Ren, T. Du, Y. Ni, H. Yan, L. Zhang, J. Sun, W. Zhang, J. Wang, A photothermal and self-induced Fenton dual-modal antibacterial platform for synergistic enhanced bacterial elimination, Appl. Catal. B Environ. 295 (2021), 120315.
[6] X. Zou, L. Zhang, Z. Wang, Y. Luo, Mechanisms of the antimicrobial activities of graphene materials, J. Am. Chem. Soc. 138 (2016) 2064–2077.
[7] J. Liu, D. Wu, N. Zhu, Y. Wu, G. Li, Antibacterial mechanisms and applications of metal-organic frameworks and their derived nanomaterials, Trends Food Sci. Technol. 109 (2021) 413–434.
[8] S. Chernousova, M. Epple, Silver as antibacterial agent: ion, nanoparticle, and metal, Angew. Chem. Int. Ed. Engl. 52 (2013) 1636–1653.
[9] Y. Tao, E. Ju, J. Ren, X. Qu, Bifunctionalized mesoporous silica-supported gold nanoparticles: intrinsic oxidase and peroxidase catalytic activities for antibacterial applications, Adv. Mater. 27 (2015) 1097–1104.
[10] F. Cao, L. Zhang, H. Wang, Y. You, Y. Wang, N. Gao, J. Ren, X. Qu, Defect-rich adhesive nanozymes as efficient antibiotics for enhanced bacterial inhibition, Angew. Chem. Int. Ed. Engl. 58 (2019) 16236–16242.
[11] D. Yang, Z. Chen, Z. Gao, S.K. Tammina, Y. Yang, Nanozymes used for antimicrobials and their applications, Colloid Surf. B 195 (2020), 111252.
[12] B. Xu, H. Wang, W. Wang, L. Gao, S. Li, X. Pan, H. Wang, H. Yang, X. Meng, Q. Wu, L. Zheng, S. Chen, X. Shi, K. Fan, X. Yan, H. Liu, A single-atom nanozyme for wound disinfection applications, Angew. Chem. Int. Ed. Engl. 58 (2019) 4911–4916.
[13] I. Thakur, B. Örmeci, A. verma, Inactivation of E. coli in water employing Fe-TiO2 composite incorporating in-situ dual process of photocatalysis and photo-Fenton in fixed-mode, J. Water Process Eng. 33 (2020), 101085.
[14] C. Liu, D. Kong, P.C. Hsu, H. Yuan, H.W. Lee, Y. Liu, H. Wang, S. Wang, K. Yan, D. Lin, P.A. Maraccini, K.M. Parker, A.B. Boehm, Y. Cui, Rapid water disinfection using vertically aligned MoS2 nanofilms and visible light, Nat. Nanotechnol. 11 (2016) 1098–1104.
[15] W. Bing, Z. Chen, H. Sun, P. Shi, N. Gao, J. Ren, X. Qu, Visible-light-driven enhanced antibacterial and biofilm elimination activity of graphitic carbon nitride by embedded Ag nanoparticles, Nano Res. 8 (2015) 1648–1658.
[16] J. Liang, F. Liu, J. Deng, M. Li, M. Tong, Efficient bacterial inactivation with Z-scheme AgI/Bi2MoO6 under visible light irradiation, Water Res. 123 (2017) 632–641.
[17] Y. Li, H. Zhou, G. Zhu, C. Shao, H. Pan, X. Xu, R. Tang, High efficient multifunctional Ag3PO4 loaded hydroxyapatite nanowires for water treatment, J. Hazard. Mater. 299 (2015) 379–387.
[18] X. Shen, R. Ma, Y. Huang, L. Chen, Z. Xu, D. Li, X. Meng, K. Fan, J. Xi, X. Yan, H. Koo, Y. Yang, J. Jiang, L. Gao, Nano-decocted ferrous polysulfide coordinates ferroptosis-like death in bacteria for anti-infection therapy, Nano Today 35 (2020), 100981.
[19] D. Han, Y. Li, X. Liu, B. Li, Y. Han, Y. Zheng, K.W.K. Yeung, C. Li, Z. Cui, Y. Liang, Z. Li, S. Zhu, X. Wang, S. Wu, Rapid bacteria trapping and killing of metal-organic frameworks strengthened photo-responsive hydrogel for rapid tissue repair of bacterial infected wounds, Chem. Eng. J. 396 (2020), 125194.
[20] J. You, Y. Guo, R. Guo, X. Liu, A review of visible light-active photocatalysts for water disinfection: features and prospects, Chem. Eng. J. 373 (2019) 624–641.
[21] Y. Tang, Z. Qin, S. Yin, H. Sun, Transition metal oxide and chalcogenide-based nanomaterials for antibacterial activities: an overview, Nanoscale 13 (2021) 6373–6388.
[22] J. Wu, X. Wang, Q. Wang, Z. Lou, S. Li, Y. Zhu, L. Qin, H. Wei, Nanomaterials with enzyme-like characteristics (nanozymes): next-generation artificial enzymes (II), Chem. Soc. Rev. 48 (2019) 1004–1076.
[23] R. Kumar, P. Raizada, N. Verma, A. Hosseini-Bandegharaei, V. Thakur, Q. Le, V. Nguyen, R. Selvasembian, P. Singh, Recent advances on water disinfection using bismuth based modified photocatalysts: strategies and challenges, J. Clean. Prod. 297 (2021), 126617.
[24] C. Liu, D. Kong, P. Hsu, H. Yuan, H. Lee, Y. Liu, H. Wang, S. Wang, K. Yan, D. Lin, P. Maraccini, K. Parker, A. Boehm, Y. Cui, Rapid water disinfection using vertically aligned MoS2 nanofilms and visible light, Nat. Nanotechnol. 11 (2016) 1098–1104.
[25] M. Agullo-Barcelo, M.I. Polo-Lopez, F. Lucena, J. Jofre, P. Fernandez-Ibanez, Solar advanced oxidation processes as disinfection tertiary treatments for real wastewater: implications for water reclamation, Appl. Catal. B Environ. 136 (2013) 341–350.
[26] L. Mei, S. Zhu, Y. Liu, W. Yin, Z. Gu, Y. Zhao, An overview of the use of nanozymes in antibacterial applications, Chem. Eng. J. 418 (2021), 129431.
[27] M. Taheri, D. Ashok, T. Sen, T.G. Enge, N.K. Verma, A. Tricoli, A. Lowe, D. R. Nisbet, T. Tsuzuki, Stability of ZIF-8 nanopowders in bacterial culture media and its implication for antibacterial properties, Chem. Eng. J. 413 (2021), 127511.
[28] X. Liu, Z. Yan, Y. Zhang, Z. Liu, Y. Sun, J. Ren, X. Qu, Two-dimensional metal-organic framework/enzyme hybrid nanocatalyst as a benign and self-activated cascade reagent for in vivo wound healing, ACS Nano 13 (2019) 5222–5230.
[29] M.A. Komkova, E.E. Karyakina, A.A. Karyakin, Catalytically synthesized prussian blue nanoparticles defeating natural enzyme peroxidase, J. Am. Chem. Soc. 140 (2018) 11302–11307.
[30] C. Abreu, Y. Nedellec, O. Ondel, F. Buret, S. Cosnier, A. Le Goff, M. Holzinger, Glucose oxidase bioanodes for glucose conversion and H2O2 production for horseradish peroxidase biocathodes in a flow through glucose biofuel cell design, J. Power Sources 392 (2018) 176–180.
[31] C. Wang, J. Fei, K. Wang, J. Li, A dipeptide-based hierarchical nanoarchitecture with enhanced catalytic activity, Angew. Chem. Int. Ed. Engl. 59 (2020) 18960–18963.
[32] Y. Wang, Y. Yang, Y. Shi, H. Song, C. Yu, Antibiotic-free antibacterial strategies enabled by nanomaterials: progress and perspectives, Adv. Mater. 32 (2020), e1904106.
[33] A.J. Huh, Y.J. Kwon, "Nanoantibiotics": a new paradigm for treating infectious diseases using nanomaterials in the antibiotics resistant era, J. Control. Release 156 (2011) 128–145.
[34] K.P. Miller, L. Wang, B.C. Benicewicz, A.W. Decho, Inorganic nanoparticles engineered to attack bacteria, Chem. Soc. Rev. 44 (2015) 7787–7807.
[35] X. Ge, S.-S. Yu, R.-F. Cheng, W. Chen, F. Zhou, K. Liang, J.-J. Chen, H.-Q. Yu, Y. Wu, Controllable drilling by corrosive Cu1Ox to access highly accessible single-site catalysts for bacterial disinfection, Appl. Catal. B Environ. 293 (2021), 120228.
[36] S. Konar, H. Kalita, N. Puvvada, S. Tantubay, M.K. Mahto, S. Biswas, A. Pathak, Shape-dependent catalytic activity of CuO nanostructures, J. Catal. 336 (2016) 11–22.
[37] L. Liu, C. Liu, H. Zhang, J. He, J. Zhai, D. Yu, S. Dong, How to identify the "LIVE/DEAD" states of microbes related to biosensing, ACS Sens. 5 (2020) 258–264.
[38] H. Dong, Y. Zuo, N. Song, S. Hong, M. Xiao, D. Zhu, J. Sun, G. Chen, C. Li, Bimetallic synergetic regulating effect on electronic structure in cobalt/vanadium co-doped carbon nitride for boosting photocatalytic performance, Appl. Catal. B Environ. 287 (2021), 119954.
[39] Q. Chen, S. Li, Y. Liu, X. Zhang, Y. Tang, H. Chai, Y. Huang, Size-controllable Fe-N/C single-atom nanozyme with exceptional oxidaselike activity for sensitive detection of alkaline phosphatase, Sens. Actuators B Chem. 305 (2020), 127511.
[40] W. Yan, S. Wang, R. Ding, X. Tian, R. Bai, H. Gang, W. Yan, Y. Xiao, F. Zhao, Long-term operation of electroactive biofilms for enhanced ciprofloxacin removal capacity and anti-shock capabilities, Bioresour. Technol. 275 (2019) 192–199.
[41] S. Jia, K. Bian, P. Shi, L. Ye, C.H. Liu, Metagenomic profiling of antibiotic resistance genes and their associations with bacterial community during multiple disinfection regimes in a full-scale drinking water treatment plant, Water Res. 176 (2020), 115721.
[42] W. Yan, R. Bai, S. Wang, X. Tian, Y. Li, S. Wang, F. Yang, Y. Xiao, X. Lu, F. Zhao, Antibiotic resistance genes are increased by combined exposure to sulfamethoxazole and naproxen but relieved by low-salinity, Environ. Int. 139 (2020), 105742.
[43] J. Tian, Q. Liu, N. Cheng, A.M. Asiri, X. Sun, Self-supported Cu3P nanowire arrays as an integrated high-performance three-dimensional cathode for generating hydrogen from water, Angew. Chem. Int. Ed. Engl. 53 (2014) 9577–9581.
[44] R. Shen, J. Xie, X. Lu, X. Chen, X. Li, Bifunctional Cu3P decorated g-C3N4 nanosheets as a highly active and robust visible-light photocatalyst for H2 production, ACS Sustain. Chem. Eng. 6 (2018) 4026–4036.
[45] C.C. Hou, Q.Q. Chen, C.J. Wang, F. Liang, Z. Lin, W.F. Fu, Y. Chen, Self-supported cedarlike semimetallic Cu3P nanoarrays as a 3D high-performance Janus Electrode for both oxygen and hydrogen evolution under basic conditions, ACS Appl. Mater. Interfaces 8 (2016) 23037–23048.
[46] F. Li, N. Li, C. Xue, H. Wang, Q. Chang, H. Liu, J. Yang, S. Hu, A Cu_2O-CDs-Cu three component catalyst for boosting oxidase-like activity with hot electrons, Chem. Eng. J. 382 (2020), 122484.
[47] F. Vetr, Z. Moradi-Shoeili, S. Özkar, Oxidation of o-phenylenediamine to 2,3-diaminophenazine in the presence of cubic ferrites MFe2O4 (M = Mn, Co, Ni, Zn) and the application in colorimetric detection of H2O2, Appl. Organomet. Chem. 32 (2018), e4465.
[48] Y. Wang, C. Chen, D. Zhang, J. Wang, Bifunctionalized novel Co-V MMO nanowires: intrinsic oxidase and peroxidase like catalytic activities for antibacterial application, Appl. Catal. B Environ. 261 (2020), 118256.
[49] W. Ma, T. Zhang, R. Li, Y. Niu, X. Yang, J. Liu, Y. Xu, C.M. Li, Bienzymatic synergism of vanadium oxide nanodots to efficiently eradicate drug-resistant bacteria during wound healing in vivo, J. Colloid Interface Sci. 559 (2020) 313–323.
[50] J. Xi, G. Wei, L. An, Z. Xu, Z. Xu, L. Fan, L. Gao, Copper/carbon hybrid nanozyme: tuning catalytic activity by the copper state for antibacterial therapy, Nano Lett. 19 (2019) 7645–7654.
[51] J. Shan, X. Li, K. Yang, W. Xiu, Q. Wen, Y. Zhang, L. Yuwen, L. Weng, Z. Teng, L. Wang, Efficient bacteria killing by Cu2WS4 nanocrystals with enzyme-like properties and bacteria-binding ability, ACS Nano 13 (2019) 13797–13808.
[52] Y. Li, Y. Li, S. Ma, P. Wang, Q. Hou, J. Han, S. Zhan, Efficient water disinfection with Ag2WO4-doped mesoporous g-C3N4 under visible light, J. Hazard. Mater. 338 (2017) 33–46.

[53] Z. Xu, Z. Qiu, Q. Liu, Y. Huang, D. Li, X. Shen, K. Fan, J. Xi, Y. Gu, Y. Tang, J. Jiang, J. Xu, J. He, X. Gao, Y. Liu, H. Koo, X. Yan, L. Gao, Converting organosulfur compounds to inorganic polysulfides against resistant bacterial infections, Nat. Commun. 9 (2018) 3713.
[54] Z. Yuan, B. Tao, Y. He, J. Liu, C. Lin, X. Shen, Y. Ding, Y. Yu, C. Mu, P. Liu, K. Cai, Biocompatible MoS2/PDA-RGD coating on titanium implant with antibacterial property via intrinsic ROS-independent oxidative stress and NIR irradiation, Biomaterials 217 (2019), 119290.
[55] Z.-Y. Huo, J.-F. Zhou, Y. Wu, Y.-H. Wu, H. Liu, N. Liu, H.-Y. Hu, X. Xie, A Cu_3P nanowire enabling high-efficiency, reliable, and energy-efficient low-voltage electroporation-inactivation of pathogens in water, J. Mater. Chem. A 6 (2018) 18813–18820.
[56] H. Jo, S. Raza, A. Farooq, J. Kim, T. Unno, Fish farm effluents as a source of antibiotic resistance gene dissemination on Jeju Island, South Korea, Environ. Pollut. 276 (2021), 116764.
[57] M. Zhang, Z. Cai, G. Zhang, Y. Zhang, N. Xue, D. Zhang, X. Pan, Effectively reducing antibiotic contamination and resistance in fishery by efficient gastrointestine-blood delivering dietary millispheres, J. Hazard. Mater. 409 (2021), 125012.
[58] Z. Shaw, S. Kuriakose, S. Cheeseman, M. Dickey, J. Genzer, A. Christofferson, R. Crawford, C. McConville, J. Chapman, V. Truong, A. Elbourne, S. Walia, Antipathogenic properties and applications of low-dimensional materials, Nat. Commun. 12 (2021) 3897.
[59] F. Qi, Y. Chang, R. Zheng, X. Wu, Y. Wu, B. Li, T. Sun, P. Wang, H. Zhang, H. Zhang, Copper phosphide nanoparticles used for combined photothermal and photodynamic tumor therapy, ACS Biomater. Sci. Eng. 7 (2021) 2745–2754.